Quaternion-Based Trajectory Optimization of Human Postures for Inducing Target Muscle Activation Patterns

Tatsuya Teramae, Takamitsu Matsubara, Tomoyuki Noda, and Jun Morimoto

***Abstract*—In exercise and rehabilitation, to effectively train the human body, human motion trajectory is essential because it induces muscle activity patterns. In this letter, we develop a novel framework for the trajectory optimization of human postures, including the head, the limbs, and the body to induce patterns of target muscle activities. Our framework has the following features: 1) a data-driven muscle-skeleton model for managing user-specific features; 2) quaternion-based state representation amenable for IMU sensors in human posture measurement; 3) joint optimization of human postures to replicate therapists who adjust not only paralyzed limbs but also patient's other limbs and body postures. We experimentally investigated the effectiveness of our framework with a shoulder joint assistive exoskeleton robot for rehabilitation.**

***Index Terms*—Quaternion, trajectory optimization, EMG, rehabilitation, physically assistive devices.**

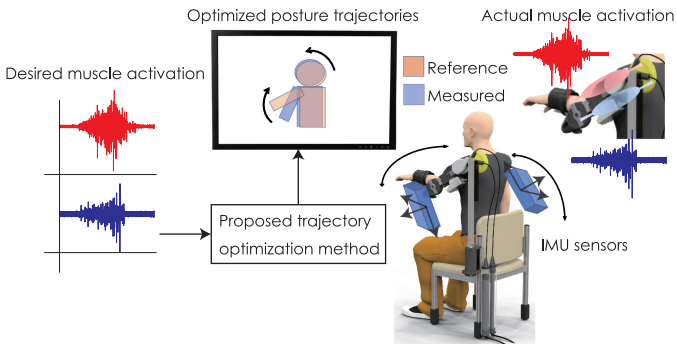

Fig. 1. Proposed concept for rehabilitation scenarios: Trajectory optimizer generates reference posture trajectories to induce desired muscle activation patterns. User tracks the optimized trajectory using visual feedback. User posture is measured by IMU sensors.

I. Introduction

MANY people worldwide are exercising to combat widespread lifestyle-related diseases. For the elderly, moderate exercise can extend their healthy life expectancy and improve their quality of life. Exercise is essential because it can effectively train human movements that induce the patterns of target muscle activities, such as types of weight training. Rehabilitation to improve physical abilities shares the same motivation. Many previous studies are based on the standardized muscle-skeleton model for modeling between muscle activation and human motion [1]–[4]. Some studies [3], [4] used a muscle-skeleton model as a joint torque estimator from electromyography (EMG). Exoskeleton-assist control was also developed [2] to induce target muscles using the muscle-skeleton model. J. Ueda *et al.* verified this controller by implementing an elbow joint exoskeleton robot in healthy participants.

Although such standardized muscle-skeleton models may be appropriate for healthy people, they might not fit the elderly and the disabled who need assistance from others or robots. In rehabilitation, the physical characteristics of stroke victims and spinal cord sufferers are different from healthy persons. Our previous studies focused on the rehabilitation of stroke patients with a shoulder exoskeleton robot [5]–[7]. We analyzed the relationship between elbow/wrist joint torque that depends on synkinesis and therapist/robot assistance during raising-arm motions in stroke patients [7]. Synkinesis denotes a patterned muscle contraction that occurs in patients with paralysis due to neuron lesions. For example, elbows and wrists bend unintentionally during arm lifting (e.g., [8]). Other clinical studies found that stroke patients have different muscle synergy patterns of synkinesis compared with healthy persons [9]–[12]. These observations suggest that a data-driven approach to generate user-specific EMG models can be more effective for rehabilitation patients than standardized models for healthy people.

Those findings motivated us to consider the problem of the trajectory optimization of human postures, including the head, the limbs, and the body to induce target muscle activation patterns for the elderly and the disabled. Our primary and specific motivation is illustrated in Fig. 1. After establishing a practical solution to this problem, an assistive-rehabilitation system could

Manuscript received February 24, 2020; accepted July 20, 2020. Date of publication August 11, 2020; date of current version August 24, 2020. This letter was recommended for publication by Associate Editor J. Pan and Editor N. Amato upon evaluation of the Reviewers' comments. This work was supported in part by the Commissioned Research of NICT, AMED under Grants JP18he0402255 and JP20he2202005 and in part by JSPS KAKENHI under Grants JP15H05321 and JP16H06565. *(Corresponding author: Tatsuya Teramae.)*

Tatsuya Teramae and Tomoyuki Noda are with the Department of Brain Robot Interface, ATR Computational Neuroscience Laboratories, Kyoto 619-0288, Japan (e-mail: t-teramae@atr.jp; t_noda@atr.jp).

Takamitsu Matsubara is with the Department of Brain Robot Interface, ATR Computational Neuroscience Laboratories, Kyoto 619-0288, Japan, and also with the Division of Information Science, Graduate School of Science and Technology, Nara Institute of Science and Technology, Ikoma 630-0192, Japan (e-mail: takam-m@is.naist.jp).

Jun Morimoto is with the Department of Brain Robot Interface, ATR Computational Neuroscience Laboratories, Kyoto 619-0288, Japan, and also with RIKEN, Tokyo 103-0027, Japan (e-mail: xmorimo@atr.jp).

Digital Object Identifier 10.1109/LRA.2020.3015460

be developed. By providing visual feedback for example references and the target trajectories of human postures, patients can perform suitable rehabilitation to induce desired target muscle activation patterns. Therefore, we focus on developing a novel framework of the trajectory optimization of human postures for inducing target muscle activation patterns with the following features:

- *Data-driven muscle-skeleton model:* To manage the user-specific characteristics of a muscle-skeleton model, as seen in elderly and disabled persons, we adopt a data-driven approach. Our model is learned from the data collected from the user. To reduce the burden of data collection, we use a probabilistic model: Sparse Pseudo-input Gaussian Processes (SPGP) [13].
- *Joint optimization of limbs and body postures:* In rehabilitation therapy, therapists often adjust the patient's *posture*, including he/her head, limbs, body, and paralyzed limbs. These adjustments induce target muscle activation patterns by suppressing synkinesis since the shoulder joint is complex and coupled with other muscles and skeletons in the trunk and waist. The therapist's adjustments were frequently observed in our previous work on rehabilitation [7].
- *Quaternion-based state representation:* We focus on Inertia Measurement Unit (IMU) sensors to measure user posture due to their high temporal resolution and accuracy, their convenient installation and easy calibration, and their required equipment compared with such optical-sensor based systems as VICON or such RGB camera-based motion capture systems as VMocap [1]. Typical IMU sensors can measure the attached frame's posture by either the Euler angles or the quaternion. However, Euler angles suffer from *gimbal lock* [14], which denotes when the angular velocity of the first and third axes diverge when the angle of the second axis becomes $\pm$ 90 degrees. Since this causes a severe problem in gradient-based optimization methods, our proposed framework instead employs quaternion-based state representation in both the muscle-skeleton model and the trajectory optimization.

The remainder of this letter is structured as follows. Section II presents our method. Section III explains our experiments that investigated its effectiveness. Section IV concludes this letter.

II. Method

Our proposed framework, which is the trajectory optimization of human postures for inducing target muscle activation patterns, consists of i) a SPGP quaternion-to-EMG model and ii) a quaternion-based trajectory optimizer (Fig. 2). The SPGP quaternion-to-EMG model is a data-driven muscle-skeleton model using SPGP that predicts EMG activation given a human posture represented by a quaternion amenable for IMUs. The SPGP quaternion-to-EMG model can be learned with data collected from the user. Its high prediction accuracy and reasonable computation cost influence the choice of using SPGP, which becomes essential for optimization. Its prediction variance can be used as a confidence measure. A quaternion-based trajectory optimizer optimizes a user-specific trajectory for inducing target muscle activation patterns using the SPGP quaternion-to-EMG model. For generating a user-friendly and rigid quaternion trajectory, our formulation is equipped with SPGP prediction variance as a cost function and a quaternion differential equation as a constraint. We jointly optimize the postures of the body and the limbs to replicate therapists who adjust not only paralyzed limbs but also the patient's other limbs and body postures. More details of each ingredient are given below.

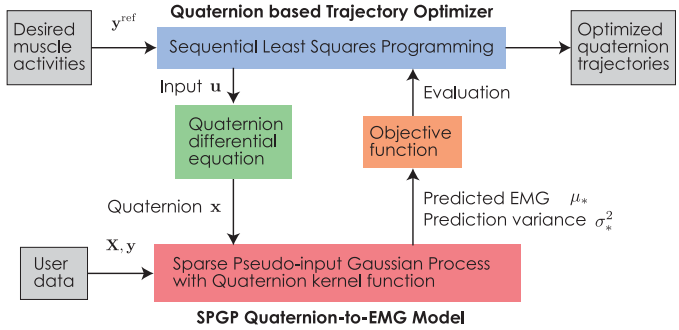

Fig. 2. Block diagram of proposed method: SPGP quaternion-to-EMG model predicts EMG activation from quaternions based on user data. Quaternion-based trajectory optimizer optimizes quaternion trajectory to induce desired EMG activation pattern.

A. SPGP Quaternion-to-EMG Model

To predict EMG signal y from set of quaternions $\mathbf{x}$ measured by IMU sensors, we assume function $y = f(\mathbf{x}) + \epsilon$, where $\epsilon \sim \mathcal{N}(0, \sigma_0^2)$ is Gaussian observation noise. $\mathbf{x}$ is composed of D IMU sensor data $[\mathbf{q}^{(1)\mathsf{T}}, \ldots, \mathbf{q}^{(D)\mathsf{T}}]^{\mathsf{T}}$, where each bit of quaternion data of one IMU sensor is denoted by $\mathbf{q} = [q_w, q_x, q_y, q_z]^{\mathsf{T}}$. Next we train this function using SPGPs with training data composed of n pairs of the quaternion and EMG data as $\mathbf{X} = \{\mathbf{x}_i\}_{i=1}^n$ and $\mathbf{y} = \{y_i\}_{i=1}^n$. Without loss of generality, we focus on one-dimensional EMG data as output, which can be easily extended to multi-dimensional output by preparing a set of multiple identical regression models.

In standard GP regression, the prior distribution of function f follows GP as $p(f|\mathbf{X}) = \mathcal{N}(f|0, \mathbf{K})$. $\mathbf{K}$ is a covariance matrix whose ij element can be defined by a kernel function as $\{\mathbf{K}_{\mathbf{x}\mathbf{x}'}\}_{ij} = k(\mathbf{x}_i, \mathbf{x}'_j)$, which measures the similarity of the inputs. By taking a likelihood function with the training data and this prior distribution into account in a Bayesian formulation, we can obtain GP predictive distribution $p(y_*|\mathbf{x}_*, \mathbf{X}, \mathbf{y}) = \mathcal{N}(y_*|\mu_*(\mathbf{x}_*), \sigma_*^2(\mathbf{x}_*))$, which can be used as a probabilistic model of function f. $\mathbf{x}_*$ and y_* are new quaternion and EMG signal. $\mu_*(\mathbf{x}_*)$ and $\sigma_*^2(\mathbf{x}_*)$ are the predictive mean and the variance of the EMG signal. However, since the calculation cost of GP prediction is $\mathcal{O}(n^2)$ by the matrix operations of data size n, the calculation cost becomes large, depending on the data size.

To alleviate this problem, Sparse Pseudo-input GP (SPGP) was proposed [13]. By using *pseudo data* to create sparse input/output space, SPGP reduces calculation costs. Given pseudo input $\bar{\mathbf{X}} = \{\bar{\mathbf{x}}_i\}_{i=1}^m$ as additional parameters, we can obtain the

following modified predictive distribution:

$$p(\mathrm{y}_*|\mathbf{x}_*, \mathbf{X}, \mathbf{y}, \bar{\mathbf{X}}) = \mathcal{N}(\mathrm{y}_*|\mu_*(\mathbf{x}_*), \sigma_*^2(\mathbf{x}_*)), \tag{1}$$

where

$$\mu_*(\mathbf{x}_*) = \mathbf{K}_{\bar{\mathbf{x}}\mathbf{x}_*}^{\mathsf{T}} \mathbf{Q}_m^{-1} \mathbf{K}_{\bar{\mathbf{x}}\mathbf{x}} (\mathbf{\Lambda} + \sigma_0^2 \boldsymbol{I})^{-1} y \tag{2}$$

$$\sigma_*^2(\mathbf{x}_*) = k(\mathbf{x}_*, \mathbf{x}_*) - \mathbf{K}_{\bar{\mathbf{x}}\mathbf{x}_*}^{\mathsf{T}} (\mathbf{K}_{\bar{\mathbf{x}}\bar{\mathbf{x}}}^{-1} - \mathbf{Q}_m^{-1}) \mathbf{K}_{\bar{\mathbf{x}}\mathbf{x}_*} + \sigma_0^2, \tag{3}$$

where $\mathbf{Q}_m = \mathbf{K}_{\bar{x}\bar{x}} + \mathbf{K}_{\bar{x}x}(\Lambda + \sigma_0^2 \mathbf{I})^{-1} \mathbf{K}_{x\bar{x}}$, $\mathbf{\Lambda} = \mathrm{diag}(\boldsymbol{\lambda})$, $\lambda_i = k(\mathbf{x}_i, \mathbf{x}_i) - \mathbf{K}_{\bar{x}\mathbf{x}_i}^{\mathsf{T}} \mathbf{K}_{\bar{x}\bar{x}}^{-1} \mathbf{K}_{\bar{x}\mathbf{x}_i}$. See reference [13] for details of the derivation. Since the calculation cost of SPGP prediction becomes $\mathcal{O}(nm)$, it reduces the calculation cost more than with standard GPs when $m < n$. We use predictive mean $\mu_*(\mathbf{x}_*)$ and variance $\sigma_*^2(\mathbf{x}_*)$ in the objective function of the quaternion trajectory optimization described in the next section.

To utilize a characteristic with quaternion data constraints on a hyper-sphere ($|\mathbf{q}|^2 = 1$), we use the quaternion kernel function with the arch distance on a hyper-sphere [15] as follows:

$$k(\mathbf{x}_i, \mathbf{x}'_j) = v^{(0)} \exp\left(-\frac{1}{2} \sum_{l=1}^{D} v^{(l)} \arccos^2(\langle \mathbf{q}_i^{(l)}, \mathbf{q}'^{(l)}_j \rangle) \right), \tag{4}$$

where

$$\langle \mathbf{q}, \mathbf{q}' \rangle = q_w q'_w + q_x q'_x + q_y q'_y + q_z q'_z. \tag{5}$$

With a marginal likelihood maximization [16], we can optimize the following hyperparameters: pseudo-input $\bar{\mathbf{X}}$ and addition noise variance σ_0^2 and kernel function parameters $v^{(0)}$ and $v^{(l)}$.

B. Quaternion-Based Trajectory Optimizer

Our trajectory optimization framework's objective is to generate the quaternion trajectory of human postures to induce target muscle activation patterns when the subject tracks optimized trajectory with visual feedback. To this end, however, two concerns arise: 1) the feasibility of the obtained trajectory for the user to follow and 2) the accuracy of the SPGP model with limited training data. If the optimized trajectory is non-smooth, users may have difficulty tracking even with visual feedback. Moreover, since the SPGP quaternion-to-EMG model is data-driven, it may result in poor prediction accuracy when the training data are insufficient.

Regarding 1), we consider the following dynamic quaternion system [17]:

$$\dot{\mathbf{x}} = \frac{1}{2} \mathbf{F}_q(\mathbf{u}) \mathbf{x}. \tag{6}$$

Mapping $\mathbf{F}_q(\mathbf{u})$ is the following block diagonal matrix $\mathbf{F}_q(\mathbf{u}) = \mathrm{blockdiag}(\mathbf{F}_q^{(1)}(\mathbf{u}), \ldots, \mathbf{F}_q^{(D)}(\mathbf{u}))$, where

$$\mathbf{F}_q^{(i)}(\mathbf{u}) = \begin{pmatrix} 0 & -\omega_x^{(i)} & -\omega_y^{(i)} & -\omega_z^{(i)} \\ \omega_x^{(i)} & 0 & \omega_z^{(i)} & -\omega_y^{(i)} \\ \omega_y^{(i)} & -\omega_z^{(i)} & 0 & \omega_x^{(i)} \\ \omega_z^{(i)} & \omega_y^{(i)} & -\omega_x^{(i)} & 0 \end{pmatrix} \tag{7}$$

is a mapping from the quaternions to their velocities where control $\mathbf{u} = [\boldsymbol{\omega}^{(1)}, \ldots, \boldsymbol{\omega}^{(D)}]$. $\boldsymbol{\omega^{(i)}} = [\omega_x^{(i)}, \omega_y^{(i)}, \omega_z^{(i)}]$, which are the three-axis angular velocities for each quaternion vector. Using this system as a constraint in optimization promotes a smooth quaternion trajectory.

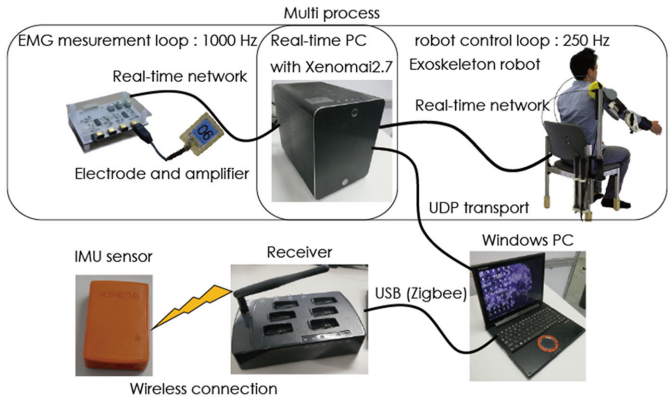

Fig. 3. Real-time robot system: Real-time OS Xenomai2.7 was installed on a real-time PC. We implemented a multi-real-time process with different control frequencies for EMG measurement and robot loop. EMG signals were measured by 1000 Hz, and robot control and sensor signals were measured by 250 Hz. EMG measurement and robot system communicated with real-time PC using a real-time UDP transport with RTnet. Real-time PC: OS: Ubuntu14.04 with Xenomai2.7, CPU: Intel(R) Core (TM) i3-7320. We wirelessly connected IMU sensor (Xsens) to a receiver, and windows PC received IMU sensor data through USB connection (Zigbee). Windows PC streamed IMU sensor data to real-time PC using UDP transport. Real-time PC received streaming data in real-time robot control loop.

Regarding 2), we utilize the prediction variance of SPGP quaternion-to-EMG model $\sigma_*^2(\mathbf{x}_*)$, since it tends to be large, depending on the scarcity of the training data around $\mathbf{x}_*$. Therefore, we minimize the prediction variance in optimization.

Finally, we formulate the trajectory optimization problem:

$$J_u = \min_{\mathbf{u}_0 \ldots \mathbf{u}_T} \sum_{i=0}^{T} \left(||\mu_*(\mathbf{x}_i) - y_i^{\mathrm{ref}}||^2 + c_v \sigma_*^2(\mathbf{x}_i) \right) \tag{8}$$

$$\text{s.t.} \quad \mathbf{x}_{i+1} = \mathbf{x}_i + \frac{1}{2} \mathbf{F}_q(\mathbf{u}_i) \mathbf{x}_i \Delta \mathrm{t} \tag{9}$$

$$\mathbf{u}_{min} < \mathbf{u} < \mathbf{u}_{max}, \tag{10}$$

where $\mathbf{y}^{\mathrm{ref}} = \{y_i^{\mathrm{ref}}\}_{i=0}^{T}$ is the target EMGs, $\Delta \mathrm{t}$ is the sampling time, and c_v is a weight coefficient. We solved this optimization problem using Sequential Least SQuares Programming (SLSQP) [18], which was implemented in a Python library (Scipy.optimization.minimize).

III. Experiment

To investigate the effectiveness of our framework, we conducted several experiments with a scenario of robotic rehabilitation (Fig. 1). Section III-A shows our robotic system with IMU and EMG sensors. Sections III-B and III-C present experimental conditions and results.

A. Robot System

This section introduces our developed robot and sensor measurement system shown in Fig. 3. We controlled the exoskeleton robot by a 250-Hz real-time loop and measured the EMG signals

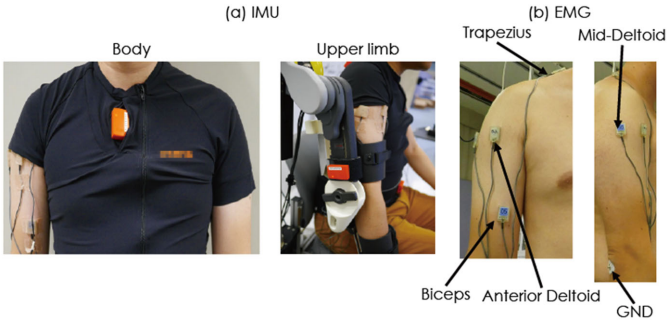

Fig. 4. Sensor conditions: (a) IMU sensors were place on body and upper limbs; (b) EMG electrodes were placed on anterior deltoid (AD), mid deltoid (MD), biceps (BB), and trapezius (Trap).

by 1000 Hz. The IMU sensor data are sent to the robot control loop by 60 Hz. We developed a shoulder exoskeleton robot for the rehabilitation of stroke patients based on clinical needs, which include safely assisting the patients with strong force to a lift-up human arm [5]. Our developed exoskeleton robot is actuated by a Pneumatic Artificial Muscle (PAM). Since PAM has a good power-weight ratio and a controllable stiffness range that is similar to a human muscle, PAM provides high affinity as an actuator for human assistance. PAM's force, which is transferred to the robot joint through a Bowden cable, can be controlled by changing its inner pressure. PAM's pressure is managed by a proportional control valve made by FESTO. The shoulder joint angle can be measured by a built-in encoder robot modular joint. The robot joint angle is limited to 0 to 90 degrees by a mechanical stopper for safety concerns. For raising-arm rehabilitation with a form that is correct for a stroke patient, the only actuated direction is the sagittal plane, and lateral rotation is suppressed by a mechanical dumper. We used an assist controller, which compensated for 25% of the gravity, at a clinical site [7]. We used a calibrated angle-to-pressure model as a robot-assistance controller. Moreover, in our previous work [7], we set for stroke patients several gains to desired pressures: 25%, 50%, 75%, and 90%. In this study, since the participants are healthy, we chose the lowest assist gain: 25%.

B. Conditions

In the experiment, we measured the subject's posture with two IMU sensors ($D = 2$) and his muscle activities with four EMG channels ($S = 4$). Fig. 4 shows the sensor placements. The EMG signals were low-pass filtered by a cutoff frequency of 3 Hz and full-wave rectification. We measured the IMU sensor and the filtered EMG data of the ten postures shown in Fig. 5 with a 25%-gravity-compensation assistance. The data of six basic postures (Fig. 5(a)–(f)) were used for training the SPGP model. The data of four combined postures (Fig. 5(g)–(j)) were used as test data for the SPGP model and the reference EMG activation pattern of the trajectory optimizer. We respectively used the posture and filtered EMG data as input and output of the target system. To obtain the EMG activation and posture data in each posture, the participant did nine raising-arm motions in each posture.

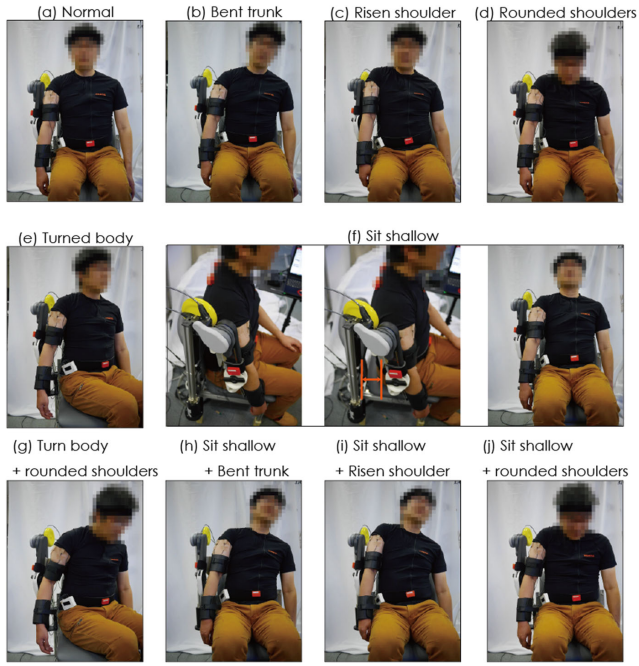

Fig. 5. Postures: (a)–(f) six basic postures and (g)–(j) four combined postures. User raises arm in each posture.

C. Results

We investigated the following four items to verify the feasibility of our proposed method:

1) *Effect of quaternion-based trajectory optimization:* We implemented our proposed system using the quaternion and Euler angles for simulated data and verified the advantage of the former for a trajectory optimization problem.
2) *Effect of quaternion kernel in the SPGP quaternion-to-EMG model:* We implemented a quaternion kernel in our model to improve its prediction accuracy. We compared SPGP's prediction accuracy with the quaternion + quaternion kernel (Eq. 4) and the Euler angle + Gaussian kernel.
3) *Quality of optimized trajectories:* We implemented the prediction variance in the objective function of the trajectory optimizer to obtain feasible quaternion trajectories for the user. To verify this term, we compared the optimized quaternion trajectories with and without the minimization term.
4) *Control performance of induced EMGs:* To verify the applicability of our proposed system for a rehabilitation scenario, we conducted an additional experiment (Fig. 1) using our framework. We compared a user's actually induced EMG activation through visual-feedback trajectory tracking with the references in the same raising-arm task.

1) Effect of Quaternion for Trajectory Optimization: To compare the performance of trajectory optimization between quaternion-based and Euler angle-based methods, we implemented a Euler angle-based optimization framework. $\mathbf{x}$ is composed of D IMU sensors as $[\boldsymbol{\theta}^{(1)}, \ldots, \boldsymbol{\theta}^{(D)}]$, where each Euler angle of one IMU sensor is denoted by $\boldsymbol{\theta}^{(i)} = [\theta_x^{(i)}, \theta_y^{(i)}, \theta_z^{(i)}]$. We used Euler dynamics $\mathbf{x}_{i+1} = \mathbf{x}_i + \mathbf{F}_E(\mathbf{x}_i)\mathbf{u}_i\Delta\mathrm{t}$ instead

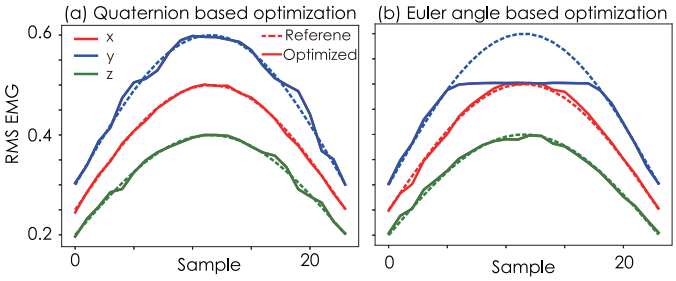

Fig. 6. Comparison of optimization results between quaternion- and Euler angle-based methods: (a) quaternion-based optimization results. (b) Euler angle-based optimization results. Solid and dotted lines represent model output and reference EMG. Red, blue, and green lines show x-, y-, and z-axes of EMG output.

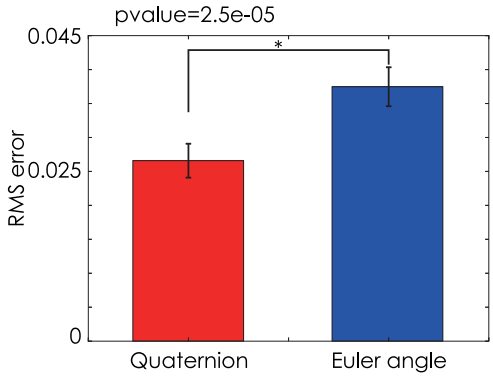

Fig. 7. Comparison of prediction error between quaternion + quaternion kernel and Euler angle + Gaussian kernel: Bar shows RMS prediction error between measured and predicted EMG. Error bar shows standard deviation. This result indicates effectiveness of quaternion kernel in our model.

of the constraint of objective function (Eq. 9), block diagonal matrix $\mathbf{F}_E(\mathbf{x}) = \mathrm{blockdiag}(\mathbf{F}_E^{(1)}(\mathbf{x}), \ldots, \mathbf{F}_E^{(D)}(\mathbf{x}))$, where

$$\mathbf{F}_E^{(i)}(\mathbf{x}) = \begin{pmatrix} 1 & \sin\theta_x^{(i)} \tan\theta_y^{(i)} & \cos\theta_x^{(i)} \\ 0 & \cos\theta_x^{(i)} & -\sin\theta_x^{(i)} \\ 0 & \frac{\sin\theta_x^{(i)}}{\cos\theta_y^{(i)}} & \frac{\cos\theta_x^{(i)}}{\cos\theta_y^{(i)}} \end{pmatrix}. \quad (11)$$

Next we prepared simulated data. We set the Euler angles to the EMG model as $\mathbf{y}_s = \frac{1}{2}\{\sin(\boldsymbol{\theta} - \frac{\pi}{2}) + 1\}$. Model output $\mathbf{y}_s$ included three EMGs associated ($S = 3$) with x-, y-, and z-axis rotation, and the input was set as a quaternion measured from one IMU sensor ($D = 1$). Reference EMG trajectories for posture optimization were set as $\mathbf{y}_i^{\mathrm{ref}} = \mathbf{C}\{\sin(\boldsymbol{\theta}^{(i)}) + \mathbf{I}\}$, where weight parameter $\mathbf{C} = [0.25, 0.3, 0.2]$ and angles $\boldsymbol{\theta}^{(i)} = \frac{\pi i}{T}\mathbf{I}$. We sampled the data around the reference EMG trajectories by adding noise that is dependent on the uniform distribution $U(-0.01, 0.01)$ and trained the SPGP model based on the training data. The duration and sampling times were set as $T = 24$ and $\Delta t = 0.01$. We set the weight parameter of the objective function (Eq. 8) to $c_v = 0.001$ and the limitations of input $\mathbf{u}_{max}$ and $\mathbf{u}_{min}$ to 200 and -200 in all the elements. We optimized the Euler angle trajectories to minimize objective function Eq. 8 based on the learned SPGP model.

Through the same procedure, we also trained the SPGP model based on the quaternion data and optimized the posture trajectories (quaternion) by conversion from the quaternion to the Euler angle in each quaternion element of all $\mathbf{x}$ using Eq. 12:

$$\begin{pmatrix} \theta_x \\ \theta_y \\ \theta_z \end{pmatrix} = \begin{pmatrix} \arctan\frac{2(q_w q_x + q_y q_z)}{q_w^2 - q_x^2 - q_y^2 + q_z^2} \\ \arcsin[2(q_w q_y - q_x q_z)] \\ \arctan\frac{2(q_w q_z + q_x q_y)}{q_w^2 + q_x^2 - q_y^2 - q_z^2} \end{pmatrix}. \quad (12)$$

Fig. 6 compares the quaternion and Euler angle-based optimization results. Fig. 6(a) shows that quaternion-based optimization follows the reference EMG trajectories. On the other hand, the EMG output of the y-axis in the Euler angle-based optimization of (b) saturates around 0.5, since the Euler angle falls to the gimbal lock (where the Euler angle of the y-axis saturates at 90 degrees). These results suggest that quaternion-based optimization is suitable for the posture optimization problem.

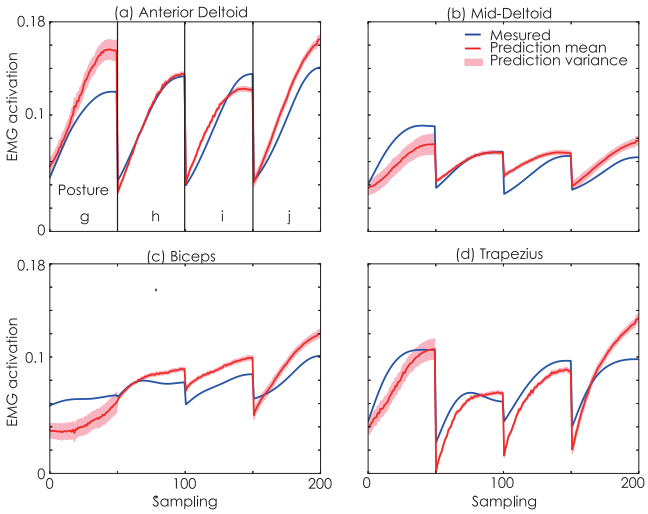

Fig. 8. EMG prediction results of SPGP: Blue lines are measured EMG activation. Red lines are predicted EMG activation by SPGP. Red region is prediction variance of SPGP. Postures g-j in graph correspond to Fig. 5(g)–(j).

2) Effect of Quaternion Kernel in the SPGP Quaternion-to-EMG Model: We compared the prediction accuracy of the SPGP quaternion-to-EMG model with the quaternion + quaternion kernel (Eq. 4) and the Euler angle + Gaussian kernel. The IMU sensor measured the quaternion and Euler angle data of the x-y-z spaces. We used the Gaussian kernel with the Euclid norm as follows: $k(\bar{\mathbf{x}}_i, \mathbf{x}_j) = v^{(0)} \exp(-\frac{1}{2}\sum_{l=1}^{D} v^{(l)} ||\bar{\mathbf{x}}_i^{(l)} - \mathbf{x}_j^{(l)}||^2)$. In the verification, we predicted the EMG activation from the quaternion data shown in the Fig. 4. We used six basic postures (Fig. 5(a)–(f)) as training data. We used four combined postures (Fig. 5 (g)(j)) as test data. Hyperparameters $v^{(0)}$ and $v^{(l)}$ of the kernel function were selected randomly, and we predicted the EMG activation of each posture using either the quaternion + quaternion kernel (Eq. 4) or the Euler angle + Gaussian kernel. We repeated this process in ten trials and calculated the prediction error between the measured EMG and the predicted activation. Fig. 7 shows the average error and the standard deviation of ten trials

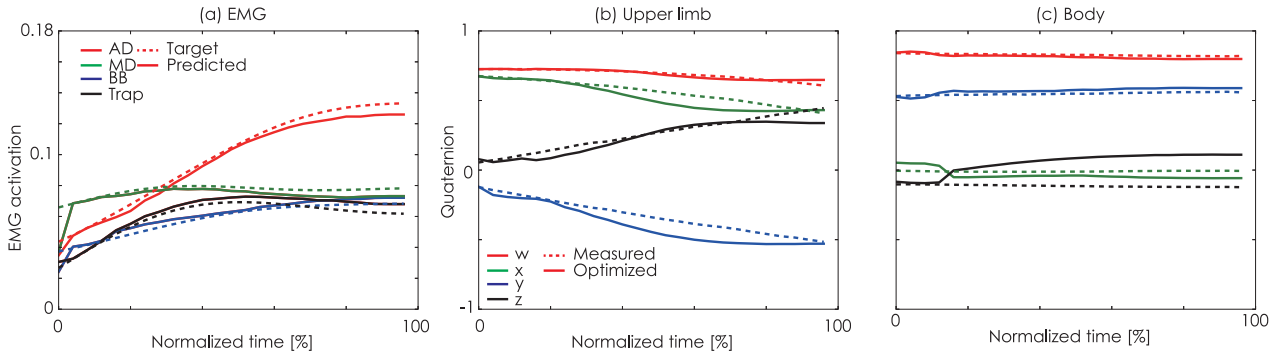

Fig. 9. Quality of optimized trajectories with minimizing prediction variance: (a) EMG activation. (b) and (c) quaternion trajectory of upper limbs and body. Dotted and solid lines represent target and predicted EMG activation in (a). Dotted and solid lines represent measured and optimized quaternion trajectory in (b) and (c).

TABLE I
RMSE BETWEEN MEASURED AND PREDICTED EMG ACTIVATION IN SPGP PREDICTION

	AD	MD	BB	Trap
Training data	0.0007	0.0003	0.0005	0.0008
Test data	0.015	0.019	0.015	0.014

using the quaternion + quaternion kernel (Eq. 4) and the Euler angle + Gaussian kernel in the test data. We tested different quaternion and Euler angles by t-test. Our result shows that the quaternion + quaternion kernel (Eq. 4) significantly improved the prediction accuracy more with the Euler angle + Gaussian kernel, suggesting that the quaternion kernel is suitable for our model. Next we optimized hyperparameters $\mathbf{v}$ of the quaternion kernel using training data (Fig. 5(a)–(f)). In this case, to reduce the computational cost, the pseudo input is the training data that were thinned out to 1/10 at equal intervals, and σ_0^2 was set 0.0001.

Fig. 8 shows the SPGP prediction results of the test data. Table I shows the Root Mean Squared Error (RMSE) of the predicted and measured EMG activation. The training data can be predicted by the EMG activation, and RMSE is small in Table I. On the other hand, the prediction of the test data has some error, and the prediction variance is larger with the training data, especially the 0-50 samples when the posture is turned body + rounded shoulder (Fig. 5(g)). Since the SPGP outputs large prediction variance when the input data are not included in the training data, the quaternion data of Fig. 5(g) have different trends with six basic postures (Fig. 5(a)–(f)). Therefore, the prediction accuracy is also lower than the other postures. However, from these characteristics, we identify the reliability of the predictions and obtain an optimized quaternion trajectory around the training data by minimizing the prediction variance. In the next section, we verify this assumption.

3) Quality of Optimized Trajectories: To verify that minimizing the prediction variance in the objective function works as a soft constraint for optimized trajectories, we set two weight parameters of objective functions (Eq. 8): 1) $c_v = 5$ and 2) $c_v = 0$. $c_v = 0$ denotes eliminating the term that minimizes the estimated variance. We set the limitation of input $\mathbf{u}_{max}$ and $\mathbf{u}_{min}$

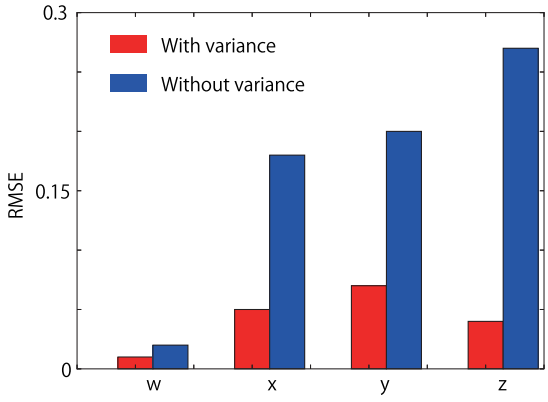

Fig. 10. RMSEs of optimized quaternion trajectory from groundtruth in upper limb IMU sensor with and without prediction variance term in the cost function. This result suggests that prediction variance in optimization generates user-friendly quaternion trajectories.

TABLE II
RMSE OF EMG ACTIVATION AND QUATERNION TRAJECTORIES IN FIGS. 9(A) AND (C)

	w	x	y	z
Proposed (body)	0.02	0.04	0.03	0.2
Without variance (body)	0.06	0.08	0.09	0.09
	AD	MD	BB	Trap
Proposed (EMG)	0.004	0.004	0.007	0.004
Without variance (EMG)	0.002	0.003	0.006	0.001

to 20 and -20 in all the elements. We also set the sampling time to $\Delta t = 0.01$ and the time duration to $T = 24$.

Fig. 9 shows the optimization results. Fig. 10 and Table II show the RMSE between the optimized motion and its groundtruth with and without prediction variance. Both methods follow the reference EMG activation pattern, but the tracking performance of the proposed method is slightly lower than the results without variance. Since weight parameter c_v has a trade-off with the tracking performance to target the EMG activation pattern, we need to carefully tune this weight. On the other hand, the optimized motion trajectories in Fig. 9 resemble the groundtruth quaternion trajectory. But in the optimization result without minimizing the prediction variance, Fig. 10 shows

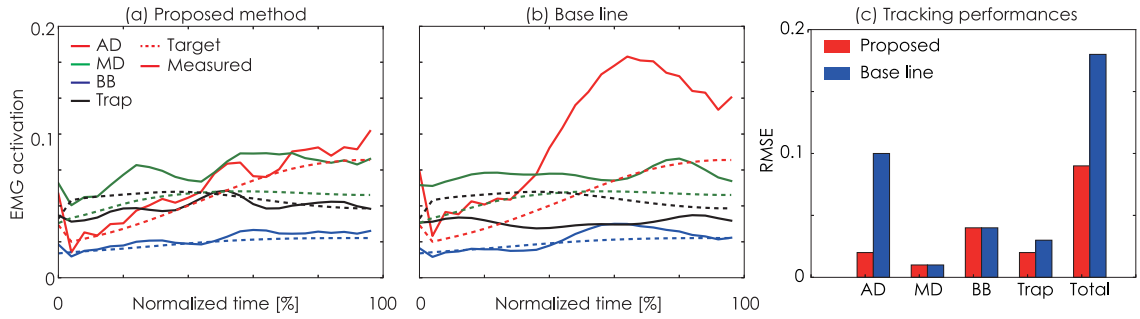

Fig. 11. Control performance of induced EMGs: (a) EMG tracking performance of proposed method and (b) base line. Dotted and solid lines represent target and ground measured EMG activation. (c) RMSEs of induced EMG activities from references: Red and blue bars show proposed method and base line. Our method resulted in fewer control errors of induced EMGs compared with base line.

TABLE III
RMSE BETWEEN REFERENCE AND MEASURED QUATERNION TRAJECTORIES IN EXPERIMENT

	w	x	y	z	Total
Proposed (upper limb)	0.16	0.11	0.06	0.12	0.45
Base line (upper limb)	0.1	0.09	0.05	0.01	0.25
Proposed method (body)	0.04	0.09	0.03	0.07	0.23
Base line (body)	0.12	0.12	0.14	0.09	0.47

Fig. 12. Human motion in experiment: actual motions when tracking reference trajectory (a) and normally raised arm (b).

that the upper limb trajectory was significantly different from the groundtruth quaternion trajectory. The quaternion trajectory tracking error of the proposed method was also smaller than the approach without prediction variance.

Those results suggest we can obtain reasonable quaternion trajectories using our proposed optimization method. Minimizing the prediction variance worked well as a soft constraint of the optimized trajectory.

4) Control Performance of Induced EMGs: We conducted an additional experiment using our framework to verify the applicability of our proposed system for a rehabilitation scenario (Fig. 1). We compared the induced EMG patterns of a user by visual-feedback trajectory tracking with the references in the same raising-arm task. We fedback the optimized trajectories as an IMU sensor rotation through a 3D animation screen. The IMU sensor rotation was fedback on the same screen. The user sees the optimized and current IMU sensor rotations. With this feedback system, the user trained himself to follow the optimized motion before the experiment. We compared the EMG activation of the optimized motion and the normal raising-arm-motion as a baseline. We set the EMG activation pattern of the sit shallow + rounded shoulder (Fig. 5(j)) posture as a target. The EMG tracking results are shown in Fig. 11. Table III shows the RMSEs of the EMG tracking and the posture trajectory tracking. Fig. 12 shows the tracking motion and the base line motion.

Fig. 11 shows that the user's induced EMG activation pattern resembles the target pattern more than the base line motion. Fig. 12 shows that the tracking result is a motion that bends the upper body, which is similar to the rounded-shoulder posture in Figs. 5(d) and (j). Table III shows that the tracking error of the body in the tracking motion is smaller than the baseline, although the upper limb is larger than the baseline, and the total tracking error was almost the same. However, the tracking motion has half the RMSE of the EMG activation compared to the baseline. These results suggest that the body's posture control is vital to induce the target EMG activation pattern.

In summary, these experimental results suggest that a user can induce a pattern of a target muscle activation using our proposed concept and system.

IV. CONCLUSION

We proposed a quaternion-based trajectory optimization method for inducing target muscle activation patterns for exercise and rehabilitation. Our experimental results suggest that our proposed method obtained reasonable quaternion trajectories using the intended objective function. Moreover, we conducted experiments to verify the applicability of our proposed system for a rehabilitation scenario and compared the measurements of the EMG activation of the tracking and regular raising-arm motions. Our experimental results show that the user induced the target EMG activation patterns using our proposed system. However, since the tracking performance was insufficient, a visual feedback system is needed to simplify following the reference trajectory.

Visualization methods of human poses using IMU and human models have been proposed [19], [20]. In the future with such techniques and tools, we will improve our visual feedback system. Although our current framework requires data collection from each user for constructing a user-specific EMG model, this requirement could be alleviated by extending it to a multi-user model that combines techniques in multi-user EMG interfaces [21], [22].

REFERENCES

[1] E. Demircan, A. Murai, O. Khatib, and Y. Nakamura, *Muscular Effort for the Characterization of Human Postural Behaviors*. Berlin, Germany: Springer, 2016, pp. 685–696.

[2] J. Ueda, D. Ming, V. Krishnamoorthy, M. Shinohara, and T. Ogasawara, "Individual muscle control using an exoskeleton robot for muscle function testing," *IEEE Trans. Neural Syst. Rehabil. Eng.*, vol. 18, no. 4, pp. 339–350, Aug. 2010.

[3] A. Erdemir, S. McLean, W. Herzog, and A. J. den Bogert, "Model-based estimation of muscle forces exerted during movements," *Clin. Biomech. (Bristol, Avon)*, vol. 22, no. 2, pp. 131–154, 2007.

[4] D. G. Lloyd and T. F. Besier, "An emg-driven musculoskeletal model to estimate muscle forces and knee joint moments in vivo," *J. Biomech.*, vol. 36, no. 6, pp. 765–776, 2003.

[5] T. Noda *et al.*, "Development of shoulder exoskeleton toward bmi triggered rehabilitation robot therapy," in *Proc. IEEE Int. Conf. Syst., Man, Cybern.*, 2018, pp. 1105–1109.

[6] M. Ogura *et al.*, "Change of muscle synergy by modulation of gravity load during shoulder flexion in patients with hemiparetic stroke. -quantitative evaluation using exoskeleton robot-," in *Proc. 13th Int. Soc. Physical Rehabil. Med. World Congr.*, 2019, p. 1.

[7] M. Hatakenaka *et al.*, "Optimizing shoulder flexion practice using an exoskeleton robot in patients with hemiparetic stroke," in *Proc. 13th Int. Soc. Physical Rehabil. Med. World Congr.*, 2019, p. 1.

[8] B. Signe, "Motor testing procedures in hemiplegia: Based on sequential recovery stages," *Physical Therapy*, vol. 46, no. 4, pp. 357–375, Apr. 1966.

[9] S. Israely, G. Leisman, C. C. Machluf, and E. Carmeli, "Muscle synergies control during hand-reaching tasks in multiple directions post-stroke," *Front Comput. Neurosci.*, vol. 12, no. 10, pp. 1–16, 2018.

[10] B. Pan *et al.*, "Alterations of muscle synergies during voluntary arm reaching movement in subacute stroke survivors at different levels of impairment," *Frontiers Comput. Neuroscience*, vol. 12, no. 69, pp. 1–11, 2018.

[11] R. L. Routson, D. J. Clark, M. G. Bowden, S. A. Kautz, and R. R. Neptune, "The influence of locomotor rehabilitation on module quality and post-stroke hemiparetic walking performance," *Gait Posture*, vol. 38, no. 3, pp. 511–517, 2013.

[12] S. Li, C. Zhuang, C. M. Niu, Y. Bao, Q. Xie, and N. Lan, "Evaluation of functional correlation of task-specific muscle synergies with motor performance in patients poststroke," *Frontiers Neurology*, vol. 8, no. 337, pp. 1–14, 2017.

[13] E. Snelson and Z. Ghahramani, "Sparse gaussian processes using pseudo-inputs," in *Advances in Neural Inf. Process. Syst. 18*, Y. Weiss, B. Schölkopf, and J. C. Platt, Eds., Cambridge, MA, USA: MIT Press, 2006, pp. 1257–1264.

[14] F. Nielsen, *Visual Computing: Geometry, Graphics, and Vision*, Charles River Media, INC., USA, 2005.

[15] M. Lang, O. Dunkley, and S. Hirche, "Gaussian process kernels for rotations and 6D rigid body motions," in *Proc. IEEE Int. Conf. Robot. Automat.*, 2014, pp. 5165–5170.

[16] M. Titsias, "Variational learning of inducing variables in sparse gaussian processes," in *Proc. 12th Int. Conf. Artif. Intell. Statist.*, 16–18 Apr. 2009, vol. 5, pp. 567–574.

[17] S. Särkkä, "Notes on quaternions," *Internal Tech. Document, Helsinki Univ. Technol.*, pp. 1–6, 2007.

[18] D. H. Kraft, *A Software Package for Sequential Quadratic Programming*. Braunschweig, Germany: Forschungsbericht-Dtsch. Forsch.-Vers. Luft-Raumfahrt (DFVLR), 1988.

[19] Y. Huang, M. Kaufmann, E. Aksan, M. J. Black, O. Hilliges, and G. Pons-Moll, "Deep inertial poser: Learning to reconstruct human pose from sparse inertial measurements in real time," *ACM Trans. Graph.*, vol. 37, no. 6, pp. 1–15, 2018.

[20] M. Loper, N. Mahmood, J. Romero, G. Pons-Moll, and M. J. Black, "SMPL: A skinned multi-person linear model," *ACM Trans. Graph.*, vol. 34, no. 6, pp. 1–16, 2015.

[21] T. Matsubara and J. Morimoto, "Bilinear modeling of EMG signals to extract user-independent features for multiuser myoelectric interface," *IEEE Trans. Biomed. Eng.*, vol. 60, no. 8, pp. 2205–2213, Aug. 2013.

[22] X. Sheng, B. Lv, W. Guo, and X. Zhu, "Common spatial-spectral analysis of EMG signals for multiday and multiuser myoelectric interface," *Biomed. Signal Process. Control*, vol. 53, 2019, Art. no. 101572.